Single Chain Structure of a

Poly(*N*-isopropylacrylamide) Surfactant in Water

Lauren J. Abbott, Ashley K. Tucker, and Mark J. Stevens[*]

Sandia National Laboratories, Albuquerque, New Mexico 87185–1395, United States

E-mail: msteve@sandia.gov

Abstract

We present atomistic simulations of a single PNIPAM-alkyl copolymer surfactant in aqueous solution at temperatures below and above the LCST of PNIPAM. We compare properties of the surfactant with pure PNIPAM oligomers of similar lengths, such as the radius of gyration and solvent accessible surface area, to determine the differences in their structures and transition behavior. We also explore changes in polymer–polymer and polymer–water interactions, including hydrogen bond formation. The expected behavior is observed in the pure PNIPAM oligomers, where the backbone folds onto itself above the LCST in order to shield the hydrophobic groups from water. The surfactant, on the other hand, does not show much conformational change as a function of temperature, but instead folds to bring the hydrophobic alkyl tail and PNIPAM head group together at all temperatures. The atomic detail available from these simulations offers important insight into understanding how the transition behavior is changed in PNIPAM-based systems.

Keywords: molecular simulations, PNIPAM, coil-to-globule transition, LCST

---
[*]To whom correspondence should be addressed

1   Introduction

Stimuli-responsive polymers undergo a structural change in response to an external stimuli (e.g., temperature, pH, light), which can be exploited for applications in drug delivery, coatings, sensors, and actuators, among others.[1–7] Polymers that are temperature responsive show conformational changes in aqueous solutions due to changes in the hydration level at different temperatures. For example, polymers with a lower critical solution temperature (LCST) exist in an extended coil state below the LCST and dehydrate or collapse into a globular state above the LCST. Poly(*N*-isopropylacrylamide) (PNIPAM) is an extensively studied thermo-responsive polymer, since it displays a sharp phase transition at its LCST around $\sim$32 °C,[8–11] near body temperature. In these amphiphilic systems, competing forces arise from the interactions of water with the hydrophilic amide groups and the hydrophobic isopropyl and backbone groups. Spectroscopy studies have suggested that the coil-to-globule transition is accompanied by a loss in polymer–water hydrogen bonds and an increase in polymer–polymer hydrogen bonds, as well as dehydration of the hydrophobic groups.[10,12–14] The dehydration of the polymer above the LCST is indicated by a significant decrease in the hydration number, as measured by various methods.[15–19] The water molecules are believed to play an important role in the transition by stabilizing the extended state below the LCST through formation of water cages and hydrogen bond bridges,[20,21] which result in severely slowed dynamics of the first hydration shell.[18,19,22]

The LCST behavior of PNIPAM can be extended to more complex architectures, such as block copolymers or surfactants, to provide responsive PNIPAM headgroups, which are useful for temperature-responsive micelle self-assembly[23–28] or nanoparticle coatings,[29–31] for example. In these types of systems, changes to the molecular weight and hydrophobic/hydrophilic balance can alter the transition behavior. Hydrophobic or hydrophilic modifications, either through copolymerization or functionalization of the side chain or backbone, have been shown to lower or raise the LCST of PNIPAM, respectively.[11,32–35] This effect becomes more important in lower molecular weight polymers, since the modifications carry greater significance. As such, although an inverse relationship is usually observed between molecular weight and the transition temperature,[36,37]

hydrophobic end groups can minimize or even reverse this trend for small chain lengths.[38–40] FitzGerald et al.,[28] for instance, showed that the transition temperature in C_{12}NIPAM surfactants was reduced up to ~20 °C when decreasing the length of the NIPAM head group. In addition to changes in the LCST, studies have also noted that the magnitude of the transition can be decreased by the addition of hydrophobic groups, presumably due to the partial aggregation or collapse of the hydrophobic segments below the LCST.[32,35] In order to exploit these types of hydrophobically modified PNIPAM-based systems, we need to improve our understanding of how the structure and transition behavior are changed correspondingly.

Molecular simulations are effective for studying the coil-to-globule transition in PNIPAM, providing molecular-level detail of the system complementary to experiments. Several studies of single chains in water have observed the expected transition behavior, although results vary depending on the force field and water model.[41–45] Some of these studies have also found a chain length dependence similar to that noted experimentally.[41,44,45] Tucker and Stevens,[45] for instance, observed a transition only in chains of length $N = 11$ or greater, but "coiling" of the chain began with $N = 30$. In addition to single PNIPAM molecules, simulations have been used to study different structural configurations like random copolymers,[46,47] graft copolymers,[43] and end-grafted brushes,[48,49] as well as different aqueous solutions incorporating salt[42] or methanol.[50] In these examples, simulations provided the molecular-level detail necessary to observe specific changes in polymer–polymer and polymer–solvent interactions,[42,44,48,50] hydrogen bonds,[43,44,47,48,50] and solvent mobility.[44,46] In one instance, Deshmukh et al.[44] even artificially "turned off" PNIPAM hydrogen bond donors and acceptors to eliminate polymer–polymer and polymer–water hydrogen bonds in the simulation, resulting in globule structures below and above the transition temperature. These examples illustrate the ability of molecular simulations to provide important insight into the transition behavior of PNIPAM and PNIPAM-based systems.

In this work, we performed molecular simulations of a single alkyl-terminated PNIPAM surfactant (PNIPAM-C18)[31] in water. There have been recent improvements in the OPLS force field for the alkane backbone, which correct the melting temperature of neat alkanes of the length we are

interested in.[51] Thus, we have also redone simulations of PNIPAM oligomers with chain lengths of $N = 8$, 18, and 30 to determine the chain length dependence of the coil-to-globule transition using the new force field parameters. The surfactant contains the same number of NIPAM monomers as the $N = 18$ oligomer and has a similar backbone length (54 carbon atoms) to the $N = 30$ oligomer (60 carbon atoms), which enables comparison between the systems. Simulations were performed for temperatures below and above the LCST of pure PNIPAM. We characterized the transition behavior of the oligomers and surfactant by the radius of gyration and solvent accessible surface area. We also explored the changes in various polymer–polymer and polymer–water interactions, including hydrogen bond formation.

2   Computational Methods

Atomistic simulations of a single PNIPAM-C18 surfactant were performed in explicit water. The surfactant studied was composed of a $C_{18}H_{37}$ alkyl tail connected to a NIPAM head of $N = 18$ monomers with a intermediary sulfur atom.[31] PNIPAM oligomers of lengths $N = 8$, 18, and 30 monomers were also considered. In all cases, the PNIPAM chains were terminated with hydrogen atoms, and only the syndiotactic state was considered, since it shows the greatest change in structure during the transition.[52–54] Interactions in the atomistic model of the polymers were described by OPLS[55] with modifications from Siu et al.,[51] and explicit water by the TIP4P/2005 model.[56] In the original OPLS-AA force field, the melting temperature of long alkanes (greater than six carbon atoms) was too high and therefore could not reproduce proper liquid properties, such that the systems would freeze in the temperature range of interest to us. Sui et al.[51] introduced new dihedral parameters that corrected this problem.

A collapsed state of the initial fully extended molecule was achieved by performing a short NVT molecular dynamics (MD) simulation in vacuum. The molecule was then surrounded by water molecules and relaxed using an energy minimization and short NVT MD simulation. Long NPT MD simulations were performed, with a minimum of 100 ns for equilibration and another 100–400

ns for production. The MD simulations were performed in GROMACS 4.6.5[57] with a leap-frog integrator and a 2 fs time step. Temperature was kept constant using a canonical thermostat[58] with a time constant of $\tau = 0.1$ ps. Pressure was kept constant at $P = 1$ bar using a Parrinello-Rahman approach[59,60] with a time constant of $\tau_P = 2$ ps. A short range Lennard–Jones and electrostatics cutoff of 1.0 nm was employed with a Verlet cutoff scheme, and long range electrostatic interactions were implemented using the Particle Mesh Ewald (PME) technique.[61] Constraints on all bonds containing hydrogen atoms were imposed using the LINCS algorithm.[62,63] Periodic boundary conditions were employed with cubic boxes of sizes $L = 4.0$ nm for the $N = 8$ oligomer, $L = 6.0$ nm for the $N = 18$ oligomer, $L = 9.0$ nm for the $N = 30$ oligomer, and $L = 7.0$ nm for the surfactant. These were chosen such that there were no interactions between periodic images.

3   Results and Discussion

We performed simulations of PNIPAM oligomers of lengths $N = 8$, 18, and 30 in water at temperatures below and above the LCST of pure PNIPAM (280 and 330 K) to determine the transition behavior captured with the revised force field, as well as to compare to the surfactant data. The extent of collapse in the chains was characterized by the radius of gyration, R_g, and solvent accessible surface area, SASA, the distributions of which are given in Figure 1. Here, the SASA was calculated in GROMACS[64] using a probe radius of 1.4 Å. Since a main driving force for the collapse of the chains is to minimize the hydrophobic surface in contact with water, the coil-to-globule transition should result in a decrease in the size of the molecule (e.g., R_g) and overall SASA. For the shortest chain length studied, $N = 8$, the R_g and SASA distributions shifted slightly to smaller values as the temperature was increased from 280 to 330 K, but no transition in the structure was observed (Figure 1a,d), as before. The chain was also simulated at 360 K, since the transition temperature is known to increase for shorter chain lengths, but still no transition was observed. This chain length is simply too short to bend and "collapse" on itself. The R_g and SASA distributions of the $N = 18$ and 30 oligomers, on the other hand, differed significantly between the temperatures,
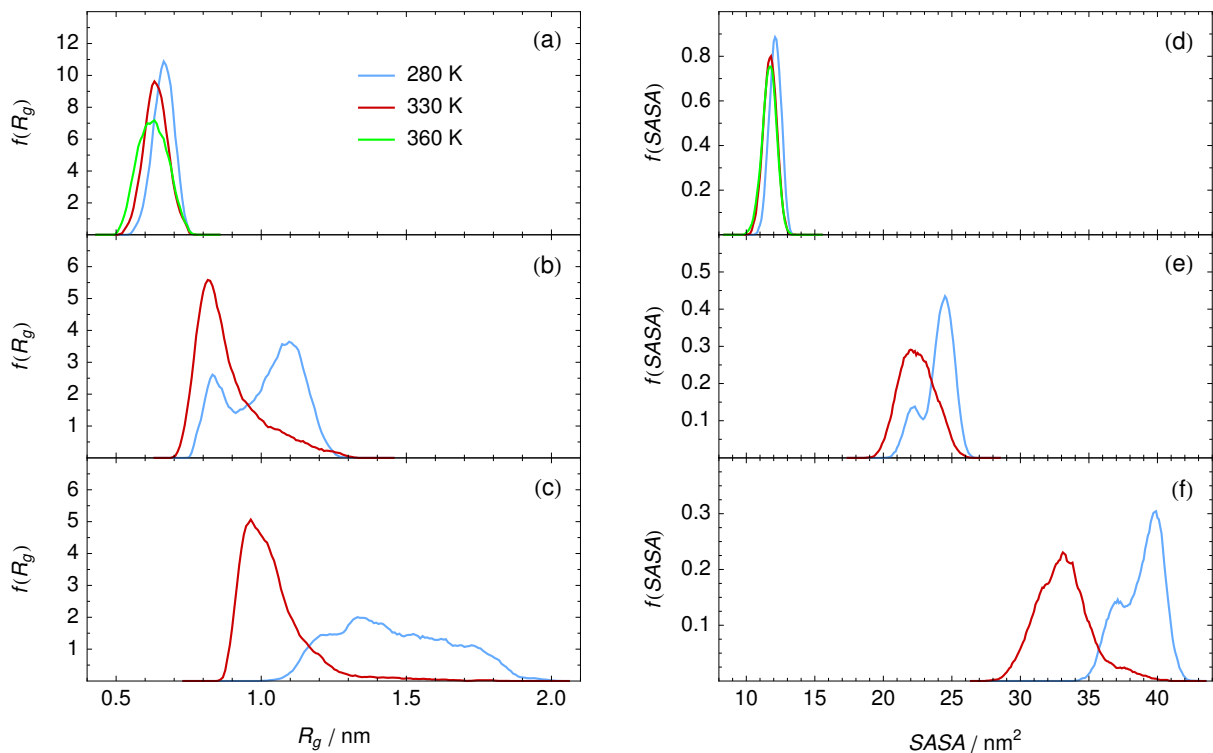
Figure 1: Distributions of the (a–c) radius of gyration, R_g, and (d–f) solvent accessible surface area, SASA, for PNIPAM oligomers of lengths $N = 8$ (top), 18 (middle), and 30 (bottom) at 280 and 330 K. Distributions at 360 K are also shown for the $N = 8$ oligomer.

indicating that these chains were long enough to explore a range of extended and (partially) collapsed structures (Figure 1b,e and c,f). The temperature difference is due to which state is primary populated; the chains were generally more extended at 280 K and more collapsed at 330 K. In addition to the distributions in Figure 1, average R_g values normalized by the average R_g at 280 K (Table 1) demonstrate how the collapse in the chains became more pronounced as the chain length was increased, similar to previous simulation studies.[41,45] Overall, these results indicate that the revised force field correctly captures the transition behavior of PNIPAM.

In order to better understand the structures, we were interested in determining the different states populated by the $N = 18$ and 30 oligomers at each temperature. The SASA appears to more directly correspond to the structural transition, since the distributions tended to be narrower than for R_g, particularly at 280 K (e.g., Figure 1c,f). Even so, the breadth of the distributions and overlapping contributions to peaks complicates the distinction of different states. Instead, density plots

Table 1: Normalized average radius of gyration, $\langle R_\mathrm{g} \rangle / \langle R_\mathrm{g}^{280} \rangle$

System	280 K	330 K
Oligomer, $N = 8$	1.00 ± 0.04	0.96 ± 0.05
Oligomer, $N = 18$	1.00 ± 0.12	0.88 ± 0.11
Oligomer, $N = 30$	1.00 ± 0.13	0.71 ± 0.08
Surfactant, all	1.00 ± 0.04	1.02 ± 0.09
Surfactant, alkyl	1.00 ± 0.11	0.97 ± 0.13
Surfactant, PNIPAM	1.00 ± 0.04	0.99 ± 0.08

of R_g versus SASA more clearly revealed two distinct states at 280 K and a single state at 330 K for the $N = 18$ and 30 oligomers, an example of which is illustrated in Figure 2. For each state at each temperature, the overall conformations of the chains were quantified by contour plots of the average distances between all monomer pairs throughout the simulations, given in Figure 3. These plots resemble protein contact maps and give some indication as to the association between different regions of the chains. For a perfectly straight chain, the plots of monomer i versus monomer j would produce contours parallel to the diagonal with an increasing separation distance moving outward from the diagonal. Any deviations from this pattern indicate bends or kinks in the chains. For the oligomers at 280 K, which showed two distinct states (e.g., Figure 2), average distance
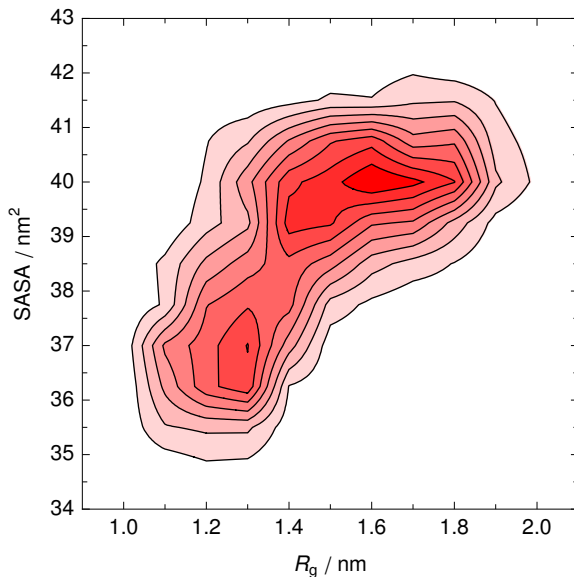

Figure 2: Density plot of the radius of gyration, R_g, versus the solvent accessible surface area, SASA, in the $N = 30$ PNIPAM oligomer at 280 K. Darker colors correspond to more populated regions.
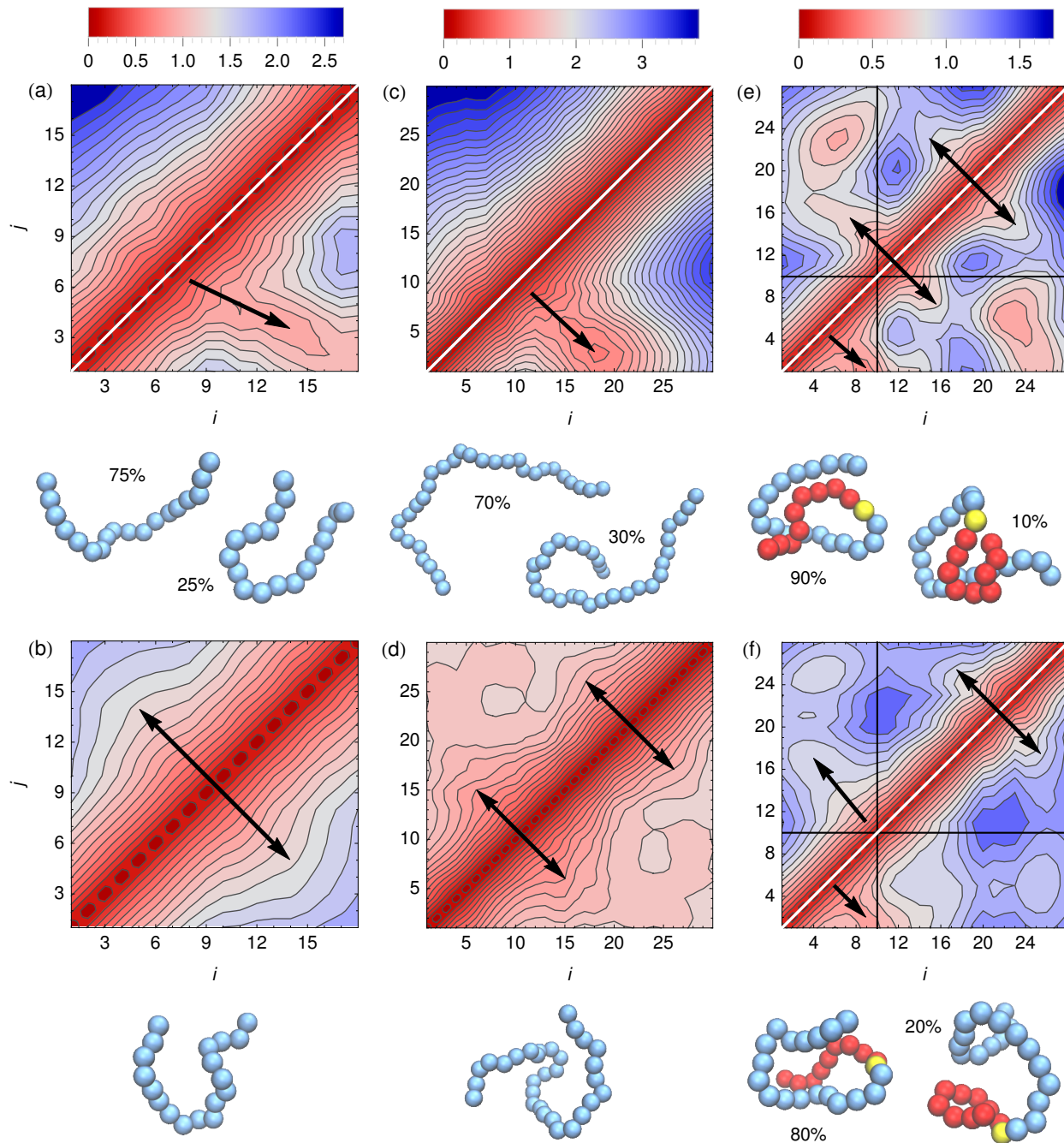
Figure 3: Contour plots showing the average distance between monomers i and j for the (a,b) $N = 18$ PNIPAM oligomer, (c,d) $N = 30$ PNIPAM oligomer, and (e,f) PNIPAM-C18 surfactant at 280 K (top) and 330 K (bottom). Bar legends at the top indicate the distances in nm. For systems with two states at a given temperature, plots are shown together, one in the upper left and one in the lower right. Black arrows are overlaid on the plots as an aid to help visualize bends in the chains (see discussion). Horizontal and vertical black lines at $i, j = 10$ in the surfactant distance maps mark the sulfur atom and distinguish the alkyl and NIPAM segments. Representative structures and their corresponding proportions are also given below each plot, where blue beads represent the NIPAM monomers, read beads the alkyl monomers, and yellow the sulfur atom.

8

maps were calculated for each state independently and are shown together with the high-R_g state in the upper left and the low-R_g state in the lower right (Figure 3a,c). In addition, representative structures were chosen for each state from a single frame in the trajectory that yielded a best fit to the average distance maps. Snapshots of these representative structures and their proportions are shown below the corresponding distance maps in Figure 3.

The $N = 18$ and 30 oligomers remained extended for the majority of the time at 280 K ($\geq 70\%$), where small-scale fluctuations of the chains averaged out and resulted in nearly parallel contours in the distance maps (upper left in Figure 3a,c). These conformations correspond to larger R_g and SASA values (Figures 1 and 2). The less common collapsed structures were indicated by peninsula-like variations in the contours extending perpendicular to the diagonal, which show that the $N = 18$ oligomer folded roughly in half (U-shaped) and the $N = 30$ oligomer at about a third (lower right in Figure 3a,c). To guide the eyes, black arrows are shown on the distance plots in Figure 3 to illustrate where the bends are visible in the contours. At 330 K, the chains were more compact, as indicated by smaller values in the distance maps overall (Figure 3b,d). Since the chains fluctuated more at the higher temperature, weaker outward deviations were observed in the contours. Thus, unlike the strong peninsula-like variations at 280 K, more subtle contours propagated outward from the points where the chains were most often bending. These bends usually occurred once at roughly the halfway point in the $N = 18$ oligomer (U-shaped) and twice into thirds in the $N = 30$ oligomer (S-shaped).

Interestingly, the corresponding segments of about 9–10 monomers is in line with the persistence length of PNIPAM.[13] In this way, the $N = 18$ oligomer populated two main states: extended (SASA ~ 25 nm^2) and collapsed with a single fold (SASA ~ 22 nm^2). The $N = 30$ oligomer, on the other hand, populated three main states: extended (SASA ~ 40 nm^2), partially collapsed with a single fold (SASA ~ 37 nm^2), and fully collapsed with two folds (SASA ~ 33 nm^2).

We found the PNIPAM-C18 surfactant data to be different than the expected temperature-responsive behavior. In Figure 4, the R_g and SASA distributions are given for the entire surfactant, as well as for specific contributions from the PNIPAM head and alkyl tail. The $N = 18$ PNIPAM
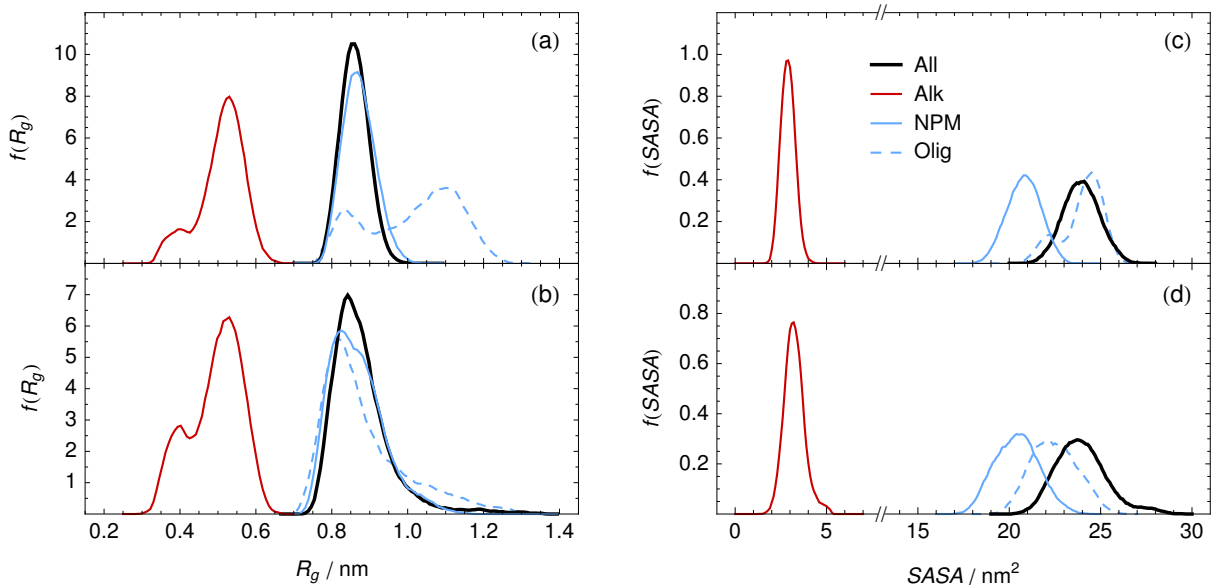
Figure 4: Distributions of the (a,b) radius of gyration, R_g, and (c,d) solvent accessible surface area, SASA, for the PNIPAM-C18 surfactant at 280 K (top) and 330 K (bottom). Note the broken x-axis in (c,d). The distributions are shown for all atoms in the molecule, as well as contributions from the alkyl tail and PNIPAM head group only. For comparison, the distributions are also given for the $N = 18$ PNIPAM oligomer (dashed lines).

oligomer data are also shown (dashed lines) for comparison with the surfactant head group. The surfactant distributions are very similar at 280 and 330 K, suggesting that the surfactant did not undergo a structural transition, unlike the $N = 18$ and 30 PNIPAM oligomers. The single peak near 0.85 nm in the R_g distributions of the PNIPAM head group at both temperatures indicates that it was in a collapsed state almost exclusively, similar to the $N = 18$ oligomer at 330 K. In comparing the PNIPAM head group of the surfactant to the pure PNIPAM oligomer, a large difference exists at 280 K. The PNIPAM oligomer has a second peak around 1.1 nm, corresponding to an extended state, which is not present for the surfactant head group. The SASA distributions for the PNIPAM head group were not similar to those of the $N = 18$ PNIPAM oligomer at either temperature, but were shifted to smaller values in both cases. This decrease is mainly due to some shielding of the PNIPAM surface by the alkyl tail. The R_g distributions of the alkyl tail suggest that it fluctuated between two states ($R_g \sim 0.4$ and 0.5 nm, respectively), however, the SASA distributions were similar at both temperatures. Overall, the R_g distributions indicate that the surfactant remained in a collapsed state at both temperatures. These results are consistent with a drop in the transition

10

temperature of the surfactant due to the addition of the hydrophobic tail, in agreement with experimental observations for hydrophobically modified NIPAM-based systems,[11,32–35] particularly the series of C_{12}NIPAM surfactants reported by FitzGerald et al.[28]

A clearer picture of the surfactant structures at both temperatures was provided by average distance maps, given in Figure 3e,f, which are divided into regions separating the alkyl tail ($i, j < 10$) and the PNIPAM head group ($i, j > 10$) at the sulfur atom (monomer 10 marked by the solid black lines). Density plots of R_g versus SASA were used to distinguish the two states observed for the alkyl tail at both temperatures (Figure 4), as was done previously. The distance maps for the two states are shown together, one in the upper left and the other in the lower right (Figure 3e,f). Because the alkyl tail is relatively short, it cannot bend easily and thus was predominantly extended at both temperatures ($\geq 80\%$) (upper left in Figure 3e,f). In these cases, the surfactant was generally bent at the sulfur atom, such that the alkyl tail is in contact with the backbone of the PNIPAM head group. On occasion, though, the surfactant was not aligned along the PNIPAM backbone, so the alkyl tail curled up into a more compact state to minimize its interactions with water (lower right in Figure 3e,f). This explains why the R_g distributions of the alkyl tail had two peaks, while only one peak was observed in the corresponding SASA distributions. At both temperatures, the PNIPAM head group was generally folded in half (U-shape). The larger fluctuations of the surfactant at 330 K resulted in weaker deviations at the bending points in the contour plots, similar to that observed for the PNIPAM oligomers. The largest difference in the temperatures was the presence of the islands in the contours corresponding to the middle of the alkyl tail and the end of the PNIPAM head group ($i, j \sim 6, 24$). This correlation was stronger at 280 K, suggesting that the alkyl tail was in contact with the PNIPAM head group more often at this temperature.

Another way to characterize the backbone–backbone interactions and hydrogen bonding is the radial distribution function (RDF), $g(r)$, which relates to the probability of finding certain atoms a distance r apart. We compared RDFs at both temperatures to determine the amount of such contacts, as shown in Figures 5 and 6. Here, 1–4 interactions and closer were excluded from the calculations. The degree to which the RDFs changed corresponded with the extent of the collapse
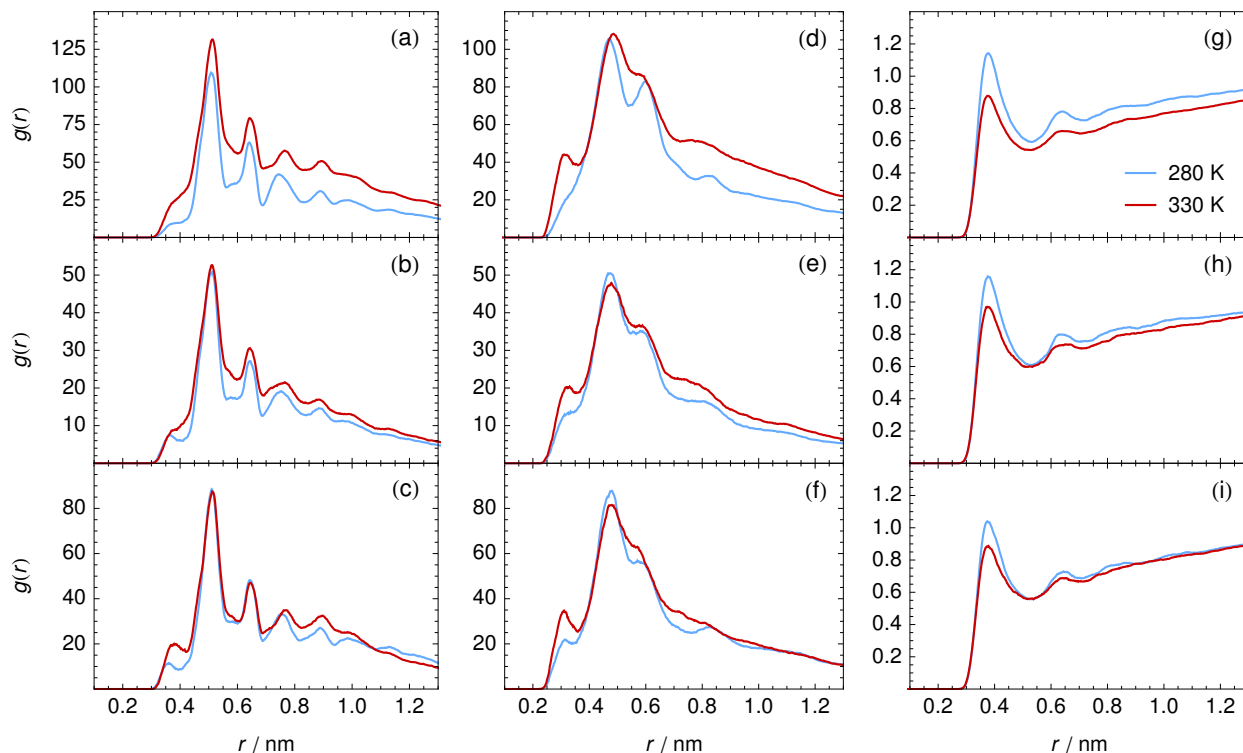
Figure 5: Radial distribution functions, $g(r)$, for (a–c) BB(npm)–BB(npm), (d–f) N–O, and (g–i) OW–CH$_3$ at 280 and 330 K, shown for the $N = 30$ PNIPAM oligomer (top), $N = 18$ PNIPAM oligomer (middle), and the PNIPAM-C18 surfactant (bottom). BB(npm) represents carbon atoms of the NIPAM backbone, N and O represent the nitrogen and oxygen atoms of the NIPAM amide groups, CH$_3$ represents the carbon atoms of the NIPAM methyl groups, and OW represents the oxygen atoms of the water molecules.

(Table 1), such that the $N = 30$ oligomer showed the greatest difference. The surfactant, which does not exhibit a structural transition, has rather small differences between the two temperatures. Generally, the RDFs showed higher peaks for polymer–polymer interactions and lower peaks for polymer–water interactions at 330 K, as expected. For example, the RDFs between NIPAM backbone carbon atoms are given in Figure 5a–c. When the backbone remained extended with mostly trans conformations, the 1–5 interactions contributed to the peak around 0.5 nm. However, the increased prevalence of gauche conformations in the more collapsed structures at 330 K yielded an increase in the number of 1–5 interactions contributing to the peak near 0.35 nm. In RDFs of the oxygen and nitrogen atoms of the NIPAM amide groups (Figure 5d–f), the intensity of the peak around 0.3 nm increased at 330 K, corresponding to the formation of more intramolecular hydrogen bonds in all cases. Conversely, the RDFs between the oxygen atoms of the water molecules
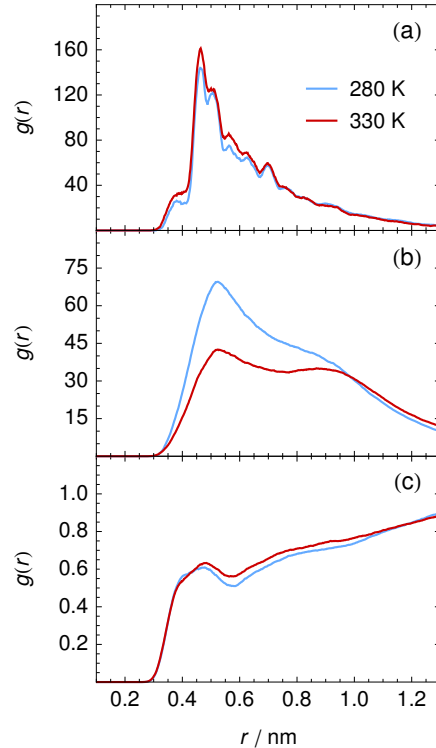
12

Figure 6: Radial distribution functions, $g(r)$, for (a) BB(alk)–BB(alk), (b) BB(alk)–BB(npm), and (c) BB(alk)–OW for the PNIPAM-C18 surfactant at 280 and 330 K. BB(alk) and BB(npm) represent carbon atoms of the alkyl and NIPAM backbone, respectively, and OW represents the oxygen atoms of the water molecules.

and the carbon atoms of the NIPAM methyl groups (Figure 5g–i) decreased, indicating dehydration of the hydrophobic groups at higher temperatures. These results are consistent with experimental data, such as shifts in IR and Raman spectra[10,12–14] and a drop in the hydration number above the transition temperature.[15–19]

The RDFs between the alkyl backbone carbon atoms, which are given in Figure 6a, are similar to those of the NIPAM backbone carbon atoms (Figure 5a–c). The slight increase in the peak near 0.35 nm indicates that more gauche conformations are formed. However, since the alkyl chain is relatively short and unable to bend easily, the change in the RDFs is minimal compared to the longer PNIPAM chains. This is in agreement with the analysis of the distance maps (Figure 3e,f), which suggested that the alkyl chains remained extended at least 80% of the time at both temperatures. Unlike all other polymer–polymer interactions in these cases, the amount of contact between the alkyl tail and PNIPAM head group decreased at 330 K, as exemplified by the RDFs of

13

the alkyl and NIPAM backbone carbon atoms in Figure 6b. The stronger 0.5 nm peak at 280 K corresponds to alkyl segments aligned closely along the PNIPAM backbone (e.g., see representative structure given in Figure 3e). These larger alkyl–PNIPAM peaks at 280 K are consistent with the more prominent islands present in the distance maps ($i, j \sim 6, 24$ in Figure 3e,f). Furthermore, the decrease in the alkyl–PNIPAM contacts at 330 K coincided with a slight increase in alkyl–water contacts, as illustrated by the RDFs of the alkyl backbone carbon atoms and the oxygen atoms of the water molecules in Figure 6c. Thus, while the PNIPAM head group made contact with itself more frequently at 330 K, the alkyl tail was pushed further away. This behavior is also visible in the representative structures of the surfactant in Figure 3e,f.

Although the RDFs provide insight into changes in general polymer–polymer and polymer–water interactions below and above the LCST of pure PNIPAM, we can directly calculate statistics of specific hydrogen bonds involving the PNIPAM amide groups and the water molecules, which are expected to play an important role in the temperature-responsive behavior of PNIPAM. Here, hydrogen bonds were measured in the simulations using criteria of $d < 3.0$ Å and $\theta > 150°$. The number of polymer–polymer and polymer–water hydrogen bonds, N_{HB}, for the entire polymer chain were measured throughout the simulations, the distributions of which are compared at both temperatures for the $N = 18$ PNIPAM oligomer and surfactant in Figure 7. For both systems, the number of polymer–polymer hydrogen bonds increased, while the number of polymer–water hydrogen bonds decreased at 330 K. The surfactant had slightly fewer polymer–water hydrogen bonds than the $N = 18$ PNIPAM oligomer at both temperatures, which suggests that the interactions of the alkyl tail with the PNIPAM head group interfered with hydrogen bond formation. In general, the large number of polymer–water hydrogen bonds present at 330 K (around two per monomer) suggests that the chain remained partially hydrated, even above the LCST of pure PNIPAM. We note, though, that a more significant dehydration would likely be observed in longer chains than the short oligomers studied here, since greater coiling could occur to produce a more compact collapsed state. Nonetheless, these results are consistent with experimental IR and Raman spectroscopy studies of PNIPAM,[10,12–14] which show the same trends and estimate that upwards
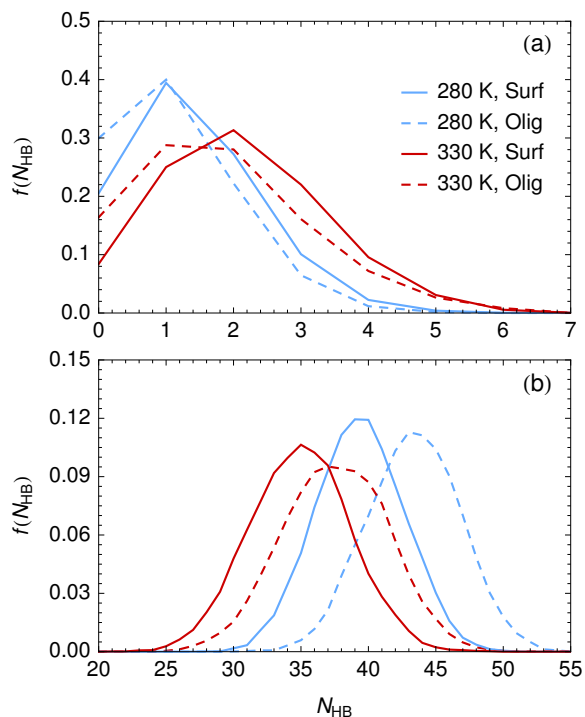
Figure 7: Distributions of (a) polymer–polymer and (b) polymer–water hydrogen bonds, N_{HB}, for the PNIPAM-C18 surfactant and the $N = 18$ PNIPAM oligomer at 280 and 330 K. Note that the total number of hydrogen bonds for the entire chain is given.

of 65% of the amide groups maintain hydrogen bonds with water.[10,12]

4   Conclusions

We have performed atomistic simulations of a PNIPAM-alkyl surfactant single chain in water at temperatures below and above the transition temperature of PNIPAM, which were compared to simulations of pure PNIPAM oligomers of similar lengths. Chain conformations were charac- terized by the radius of gyration and solvent accessible surface area, which both decrease in the collapsed state as the chain folds to minimize the amount of hydrophobic surface in contact with water. Additionally, average distance maps were calculated for the states observed at both tempera- tures to identify common associations between different regions of the chains. Unlike the PNIPAM oligomers, the surfactant did not show temperature-responsive behavior, but instead existed in a collapsed state at both temperatures. These findings suggest a decrease in the transition tempera-

ture of the surfactant due to the addition of the hydrophobic tail, which is consistent with experimental studies of similar systems. In all cases, folding of the PNIPAM chain occurred in segments of roughly 9–10 monomers in correspondence with the persistence length of PNIPAM. Generally, polymer–polymer contacts increased, while polymer–water contacts decreased above the LCST of pure PNIPAM. Similar trends were also observed for polymer–polymer and polymer–water hydrogen bonds among the PNIPAM amide groups and water molecules. Even in the collapsed state, there were a large number of polymer–water hydrogen bonds, suggesting that the PNIPAM chains remained partially hydrated.

Competing forces exist in these amphiphilic PNIPAM systems, where the chain conformation tries to maximize favorable interactions between water and the hydrophilic amide groups (e.g., through hydrogen bonds), while at the same time minimizing the exposure of the hydrophobic isopropyl and backbone groups to water. The addition of the hydrophobic alkyl tail in the surfactant alters the hydrophobic/hydrophilic balance and is thus a key factor in its nonresponsive behavior. Since having the alkyl tail alone in water is highly unfavorable, the surfactant collapses to bring the tail in contact with to the PNIPAM backbone both below and above the transition temperature of PNIPAM. In the collapsed state, therefore, the surface of the hydrophobic groups is more effectively shielded from the water. Despite the results presented here for a single surfactant in water, it is important to point out that temperature-responsive behavior could be achieved still for PNIPAM-based surfactants. For example, increasing the size of the PNIPAM head group relative to the hydrophobic tail might allow a coil-to-globule transition to occur in a portion of the PNIPAM segment further away from the hydrophobic tail. Additionally, the behavior of these types of surfactants may differ when aggregates (e.g., micelles) are formed, since interactions between multiple hydrophobic tails may lead to fewer interactions with the PNIPAM head groups. Further studies are needed to understand how the temperature-responsive behavior is affected in these instances.

Acknowledgement

References

(1) Stuart, M. A. C. et al. Emerging Applications of Stimuli-Responsive Polymer Materials. *Nat. Mater.* **2010**, *9*, 101–113.

(2) Liu, F.; Urban, M. W. Recent Advances and Challenges in Designing Stimuli-Responsive Polymers. *Prog. Polym. Sci.* **2010**, *35*, 3–23.

(3) Cayre, O. J.; Chagneux, N.; Biggs, S. Stimulus Responsive Core-Shell Nanoparticles: Synthesis and Applications of Polymer Based Aqueous Systems. *Soft Matter* **2011**, *7*, 2211–2234.

(4) Fleige, E.; Quadir, M. A.; Haag, R. Stimuli-Responsive Polymeric Nanocarriers for the Controlled Transport of Active Compounds: Concepts and Applications. *Adv. Drug Deliv. Rev.* **2012**, *64*, 866–884.

(5) Lee, S.-M.; Nguyen, S. T. Smart Nanoscale Drug Delivery Platforms from Stimuli-Responsive Polymers and Liposomes. *Macromolecules* **2013**, *46*, 9169–9180.

(6) Roy, D.; Brooks, W. L. A.; Sumerlin, B. S. New Directions in Thermoresponsive Polymers. *Chem. Soc. Rev.* **2013**, *42*, 7214–7243.

(7) Zhai, L. Stimuli-Responsive Polymer Films. *Chem. Soc. Rev.* **2013**, *42*, 7148–7160.

(8) Otake, K.; Inomata, H.; Konno, M.; Saito, S. Thermal Analysis of the Volume Phase Transition with N-isopropylacrylamide Gels. *Macromolecules* **1990**, *23*, 283–289.

(9) Wu, C.; Zhou, S. Laser Light Scattering Study of the Phase Transition of Poly(N-isopropylacrylamide) in Water. 1. Single Chain. *Macromolecules* **1995**, *28*, 8381–8387.

(10) Maeda, Y.; Higuchi, T.; Ikeda, I. Change in Hydration State during the Coil–Globule Transition of Aqueous Solutions of Poly(N-isopropylacrylamide) as Evidenced by FTIR Spectroscopy. *Langmuir* **2000**, *16*, 7503–7509.

(11) Kujawa, P.; Winnik, F. M. Volumetric Studies of Aqueous Polymer Solutions Using Pressure Perturbation Calorimetry: A New Look at the Temperature-Induced Phase Transition of Poly(N-isopropylacrylamide) in Water and D_2O. *Macromolecules* **2001**, *34*, 4130–4135.

(12) Sun, B.; Lin, Y.; Wu, P.; Siesler, H. W. A FTIR and 2D-IR Spectroscopic Study on the Microdynamics Phase Separation Mechanism of the Poly(N-isopropylacrylamide) Aqueous Solution. *Macromolecules* **2008**, *41*, 1512–1520.

(13) Ahmed, Z.; Gooding, E. A.; Pimenov, K. V.; Wang, L.; Asher, S. A. UV Resonance Raman Determination of Molecular Mechanism of Poly(N-isopropylacrylamide) Volume Phase Transition. *J. Phys. Chem. B* **2009**, *113*, 4248–4256.

(14) Lai, H.; Wu, P. A Infrared Spectroscopic Study on the Mechanism of Temperature-Induced Phase Transition of Concentrated Aqueous Solutions of Poly(N-isopropylacrylamide) and N-isopropylpropionamide. *Polymer* **2010**, *51*, 1404–1412.

(15) Kogure, H.; Nanami, S.; Masuda, Y.; Toyama, Y.; Kubota, K. Hydration and Dehydration Behavior of N-isopropylacrylamide Gel Particles. *Colloid Polym. Sci.* **2005**, *283*, 1163–1171.

(16) Ono, Y.; Shikata, T. Hydration and Dynamic Behavior of Poly(N-isopropylacrylamide)s in Aqueous Solution: A Sharp Phase Transition at the Lower Critical Solution Temperature. *J. Am. Chem. Soc.* **2006**, *128*, 10030–10031.

(17) Satokawa, Y.; Shikata, T.; Tanaka, F.; Qiu, X.-p.; Winnik, F. M. Hydration and Dynamic Behavior of a Cyclic Poly(N-isopropylacrylamide) in Aqueous Solution: Effects of the Polymer Chain Topology. *Macromolecules* **2009**, *42*, 1400–1403.

(18) Füllbrandt, M.; Ermilova, E.; Asadujjaman, A.; Hölzel, R.; Bier, F. F.; von Klitzing, R.; Schönhals, A. Dynamics of Linear Poly(N-isopropylacrylamide) in Water Around the Phase Transition Investigated by Dielectric Relaxation Spectroscopy. *J. Phys. Chem. B* **2014**, *118*, 3750–3759.

(19) Philipp, M.; Kyriakos, K.; Silvi, L.; Lohstroh, W.; Petry, W.; Krüger, J. K.; Papadakis, C. M.; Müller-Buschbaum, P. From Molecular Dehydration to Excess Volumes of Phase-Separating PNIPAM Solutions. *J. Phys. Chem. B* **2014**, *118*, 4253–4260.

(20) Cho, E. C.; Lee, J.; Cho, K. Role of Bound Water and Hydrophobic Interaction in Phase Transition of Poly(N-isopropylacrylamide) Aqueous Solution. *Macromolecules* **2003**, *36*, 9929–9934.

(21) Ono, Y.; Shikata, T. Contrary Hydration Behavior of N-isopropylacrylamide to its Polymer, P(NIPAm), with a Lower Critical Solution Temperature. *J. Phys. Chem. B* **2007**, *111*, 1511–1513.

(22) Alam, T. M.; Childress, K. K.; Pastoor, K.; Rice, C. V. Characterization of Free, Restricted, and Entrapped Water Environments in Poly(N-isopropyl acrylamide) hydrogels via ^{1}H HRMAS PFG NMR Spectroscopy. *J. Polym. Sci., Part B* **2014**, *52*, 1521–1527.

(23) Winnik, F. M.; Davidson, A. R.; Hamer, G. K.; Kitano, H. Amphiphilic Poly(N-isopropylacrylamides) Prepared by Using a Lipophilic Radical Initiator: Synthesis and Solution Properties in Water. *Macromolecules* **1992**, *25*, 1876–1880.

(24) Chung, J. E.; Yokoyama, M.; Suzuki, K.; Aoyagi, T.; Sakurai, Y.; Okano, T. Reversibly Thermo-Responsive Alkyl-Terminated Poly(N-isopropylacrylamide) Core-Shell Micellar Structures. *Colloids Surf., B* **1997**, *9*, 37–48.

(25) Koga, T.; Tanaka, F.; Motokawa, R.; Koizumi, S.; Winnik, F. M. Theoretical Modelling of Hierarchically Associated Structures in Hydrophobically Modified PNIPAM Aqueous Solutions on the Basis of a Neutron Scattering Study. *Macromol. Symp.* **2010**, *291–292*, 177–185.

(26) Du, B.; Mei, A.; Yang, Y.; Zhang, Q.; Wang, Q.; Xu, J.; Fan, Z. Synthesis and Micelle Behavior of (PNIPAm-PtBA-PNIPAm)m Amphiphilic Multiblock Copolymer. *Polymer* **2010**, *51*, 3493–3502.

(27) Adelsberger, J.; Meier-Koll, A.; Bivigou-Koumba, A. M.; Busch, P.; Holderer, O.; Hellweg, T.; Laschewsky, A.; Müller-Buschbaum, P.; Papadakis, C. M. The Collapse Transition and the Segmental Dynamics in Concentrated Micellar Solutions of P(S-b-NIPAM) Diblock Copolymers. *Colloid Polym. Sci.* **2011**, *289*, 711–720.

(28) FitzGerald, P. A.; Gupta, S.; Wood, K.; Perrier, S.; Warr, G. G. Temperature- and pH-Responsive Micelles with Collapsible Poly(N-isopropylacrylamide) Headgroups. *Langmuir* **2014**, *30*, 7986–7992.

(29) Nuopponen, M.; Tenhu, H. Gold Nanoparticles Protected with pH and Temperature-Sensitive Diblock Copolymers. *Langmuir* **2007**, *23*, 5352–5357.

(30) Liu, J.; Li, A.; Tang, J.; Wang, R.; Kong, N.; Davis, T. P. Thermoresponsive Silver/Polymer Nanohybrids with Switchable Metal Enhanced Fluorescence. *Chem. Comm.* **2012**, *48*, 4680–4682.

(31) Li, B.; Smilgies, D.-M.; Price, A. D.; Huber, D. L.; Clem, P. G.; Fan, H. Poly(N-isopropylacrylamide) Surfactant-Functionalized Responsive Silver Nanoparticles and Superlattices. *ACS Nano* **2014**, *8*, 4799–4804.

(32) Chee, C. K.; Rimmer, S.; Shaw, D. A.; Soutar, I.; Swanson, L. Manipulating the Thermoresponsive Behavior of Poly(N-isopropylacrylamide). 1. On the Conformational Behavior of a Series of N-Isopropylacrylamide–Styrene Statistical Copolymers. *Macromolecules* **2001**, *34*, 7544–7549.

(33) Siu, M.; Zhang, G.; Wu, C. Effect of Comonomer Distribution on the Coil-to-Globule Transition of a Single AB Copolymer Chain in Dilute Solution. *Macromolecules* **2002**, *35*, 2723–2727.

(34) Cao, Z.; Liu, W.; Gao, P.; Yao, K.; Li, H.; Wang, G. Toward an Understanding of Thermoresponsive Transition Behavior of Hydrophobically Modified N-isopropylacrylamide Copolymer Solution. *Polymer* **2005**, *46*, 5268–5277.

(35) Rimmer, S.; Soutar, I.; Swanson, L. Switching the Conformational Behaviour of Poly(N-isopropyl acrylamide). *Polym. Int.* **2009**, *58*, 273–278.

(36) Xia, Y.; Yin, X.; Burke, N. A. D.; Stöver, H. D. H. Thermal Response of Narrow-Disperse Poly(N-isopropylacrylamide) Prepared by Atom Transfer Radical Polymerization. *Macromolecules* **2005**, *38*, 5937–5943.

(37) Shan, J.; Zhao, Y.; Granqvist, N.; Tenhu, H. Thermoresponsive Properties of N-Isopropylacrylamide Oligomer Brushes Grafted to Gold Nanoparticles: Effects of Molar Mass and Gold Core Size. *Macromolecules* **2009**, *42*, 2696–2701.

(38) Xia, Y.; Burke, N. A. D.; Stöver, H. D. H. End Group Effect on the Thermal Response of Narrow-Disperse Poly(N-isopropylacrylamide) Prepared by Atom Transfer Radical Polymerization. *Macromolecules* **2006**, *39*, 2275–2283.

(39) Furyk, S.; Zhang, Y.; Ortiz-Acosta, D.; Cremer, P. S.; Bergbreiter, D. E. Effects of End Group Polarity and Molecular Weight on the Lower Critical Solution Temperature of Poly(N-isopropylacrylamide). *J. Polym. Sci., Part A* **2006**, *44*, 1492–1501.

(40) Duan, Q.; Miura, Y.; Narumi, A.; Shen, X.; Sato, S.-I.; Satoh, T.; Kakuchi, T. Synthesis and Thermoresponsive Property of End-Functionalized Poly(N-isopropylacrylamide) with Pyrenyl Group. *J. Polym. Sci., Part A* **2006**, *44*, 1117–1124.

(41) Walter, J.; Ermatchkov, V.; Vrabec, J.; Hasse, H. Molecular Dynamics and Experimental Study of Conformation Change of Poly(N-isopropylacrylamide) Hydrogels in Water. *Fluid Phase Equilib.* **2010**, *296*, 164–172.

(42) Du, H.; Wickramasinghe, R.; Qian, X. Effects of Salt on the Lower Critical Solution Temperature of Poly(N-isopropylacrylamide). *J. Phys. Chem. B* **2010**, *114*, 16594–16604.

(43) Chiessi, E.; Lonardi, A.; Paradossi, G. Toward Modeling Thermoresponsive Polymer Networks: A Molecular Dynamics Simulation Study of N-isopropyl Acrylamide Co-Oligomers. *J. Phys. Chem. B* **2010**, *114*, 8301–8312.

(44) Deshmukh, S. A.; Sankaranarayanan, S. K. R. S.; Suthar, K.; Mancini, D. C. Role of Solvation Dynamics and Local Ordering of Water in Inducing Conformational Transitions in Poly(N-isopropylacrylamide) Oligomers Through the LCST. *J. Phys. Chem. B* **2012**, *116*, 2651–2663.

(45) Tucker, A. K.; Stevens, M. J. Study of the Polymer Length Dependence of the Single Chain Transition Temperature in Syndiotactic Poly(N-isopropylacrylamide) Oligomers in Water. *Macromolecules* **2012**, *45*, 6697–6703.

(46) Gangemi, F.; Longhi, G.; Abbate, S.; Lebon, F.; Cordone, R.; Ghilardi, G. P.; Fornili, S. L. Molecular Dynamics Simulation of Aqueous Solutions of 26-Unit Segments of p(NIPAAm) and of p(NIPAAm) "Doped" with Amino Acid Based Comonomers. *J. Phys. Chem. B* **2008**, *112*, 11896–11906.

(47) Liu, M. S.; Taylor, C.; Chong, B.; Liu, L.; Bilic, A.; Terefe, N. S.; Stockmann, R.; Thang, S. H.; Silva, K. D. Conformational Transitions and Dynamics of Thermal Responsive Poly(N-isopropylacrylamide) Polymers as Revealed by Molecular Simulation. *Eur. Polym. J.* **2014**, *55*, 153–159.

(48) Lee, S. G.; Pascal, T. A.; Koh, W.; Brunello, G. F.; Goddard, W. A.; Jang, S. S. Deswelling

Mechanisms of Surface-Grafted Poly(NIPAAm) Brush: Molecular Dynamics Simulation Approach. *J. Phys. Chem. C* **2012**, *116*, 15974–15985.

(49) Lorbeer, L.; Alaghemandi, M.; Spohr, E. Molecular Dynamics Studies of Poly(N-isopropylacrylamide) Endgrafted on the Surfaces of Model Slab Pores. *J. Mol. Liq.* **2014**, *189*, 57–62.

(50) Pang, J.; Yang, H.; Ma, J.; Cheng, R. Solvation Behaviors of N-isopropylacrylamide in Water/Methanol Mixtures Revealed by Molecular Dynamics Simulations. *J. Phys. Chem. B* **2010**, *114*, 8652–8658.

(51) Siu, S. W. I.; Pluhackova, K.; Böckmann, R. A. Optimization of the OPLS-AA Force Field for Long Hydrocarbons. *J. Chem. Theory Comput.* **2012**, *8*, 1459–1470.

(52) Ray, B.; Okamoto, Y.; Kamigaito, M.; Sawamoto, M.; Seno, K.-i.; Kanaoka, S.; Aoshima, S. Effect of Tacticity of Poly(N-isopropylacrylamide) on the Phase Separation Temperature of its Aqueous Solutions. *Polym. J.* **2005**, *37*, 234–237.

(53) Katsumoto, Y.; Kubosaki, N. Tacticity Effects on the Phase Diagram for Poly(N-isopropylacrylamide) in Water. *Macromolecules* **2008**, *41*, 5955–5956.

(54) Autieri, E.; Chiessi, E.; Lonardi, A.; Paradossi, G.; Sega, M. Conformation and Dynamics of Poly(N-isopropyl acrylamide) Trimers in Water: A Molecular Dynamics and Metadynamics Simulation Study. *J. Phys. Chem. B* **2011**, *115*, 5827–5839.

(55) Jorgensen, W. L.; Maxwell, D. S.; Tirado-Rives, J. Development and Testing of the OPLS All-Atom Force Field on Conformational Energetics and Properties of Organic Liquids. *J. Am. Chem. Soc.* **1996**, *118*, 11225–11236.

(56) Abascal, J. L. F.; Vega, C. A General Purpose Model for the Condensed Phases of Water: TIP4P/2005. *J. Chem. Phys.* **2005**, *123*, 234505.

(57) Pronk, S. et al. GROMACS 4.5: A High-Throughput and Highly Parallel Open Source Molecular Simulation Toolkit. *Bioinformatics* **2013**, *29*, 845–854.

(58) Bussi, G.; Donadio, D.; Parrinello, M. Canonical Sampling Through Velocity Rescaling. *J. Chem. Phys.* **2007**, *126*, 014101.

(59) Parrinello, M.; Rahman, A. Polymorphic Transitions in Single Crystals: A New Molecular Dynamics Method. *J. Appl. Phys.* **1981**, *52*, 7182–7190.

(60) Nosé, S.; Klein, M. L. Constant Pressure Molecular Dynamics for Molecular Systems. *Mol. Phys.* **1983**, *50*, 1055–1076.

(61) Darden, T.; York, D.; Pedersen, L. Particle Mesh Ewald: An N log(N) Method for Ewald Sums in Large Systems. *J. Chem. Phys.* **1993**, *98*, 10089–10092.

(62) Hess, B.; Bekker, H.; Berendsen, H. J. C.; Fraaije, J. G. E. M. LINCS: A Linear Constraint Solver for Molecular Simulations. *J. Comput. Chem.* **1997**, *18*, 1463–1472.

(63) Hess, B. P-LINCS: A Parallel Linear Constraint Solver for Molecular Simulation. *J. Chem. Theory Comput.* **2008**, *4*, 116–122.

(64) Eisenhaber, F.; Lijnzaad, P.; Argos, P.; Sander, C.; Scharf, M. The Double Cubic Lattice Method: Efficient Approaches to Numerical Integration of Surface Area and Volume and to Dot Surface Contouring of Molecular Assemblies. *J. Comput. Chem.* **1994**, *16*, 273–284.

TOC Graphic

T < LCST

Oligomer   Surfactant

T > LCST